Diamond & Related Materials 145 (2024) 111149

Contents lists available at ScienceDirect

Diamond & Related Materials

journal homepage: www.elsevier.com/locate/diamond

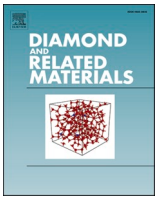

Synergistic effect of graphene and nanodiamonds to achieve ultra-low friction on rough DLC coatings

Andrea Mescola [a], Alessia Lodi [b], Federico Zanni [b], Alberto Rota [a,b,c], Andrea Gerbi [d], Cristina Bernini [d], Marine Schott [e], Luca Repetto [e], Adalberto Camisasca [f], Silvia Giordani [f], Renato Buzio [d,*], Guido Paolicelli [a,*]

[a] CNR-NANO Istituto Nanoscienze, Via Campi 213/a, 41125 Modena, Italy
[b] FIM, Dipartimento di Scienze Fisiche, Informatiche e Matematiche, Università di Modena e Reggio Emilia, Via Campi 213/A, 41125 Modena, Italy
[c] Centro Interdipartimentale per la Ricerca Applicata e i Servizi nella Meccanica Avanzata e nella Motoristica Intermech-Mo.Re, Università di Modena e Reggio Emilia, Via Vignolese 905/b, 41125 Modena, Italy
[d] CNR-SPIN Institute for Superconductors, Innovative Materials and Devices, Corso F.M. Perrone 24, 16152 Genova, Italy
[e] Department of Physics, Università di Genova, Via Dodecaneso, 33, 16146 Genova, Italy
[f] School of Chemical Sciences, Dublin City University, Glasnevin, Dublin D09 NA55, Ireland

ARTICLE INFO

Keywords:
Diamond-like carbon (DLC)
Graphene
Nanodiamonds
Ultra-low friction
Raman spectroscopy

ABSTRACT

Diamond-like carbon (DLC) with its protective, antiwear and self-lubricant properties represents an outstanding coating material to improve the tribological performance of bare metal-to-metal contacts. The DLC friction response is strictly related to the generation of a carbon-rich transfer layer on the sliding countersurfaces. This key process may benefit from the DLC surface functionalization with carbon nanomaterials, as attested by the recent observation of wearless sliding and ultra-low friction for nanorough model interfaces. In this study, we show by ball-on-disc tribometer that the tribological response of microrough steel-DLC contacts is considerably improved in dry atmosphere through DLC functionalization with graphene sheets (GSs) and nanodiamonds (NDs). The functionalization effectiveness is demonstrated exclusively with both allotropic forms, that synergically lower friction after a unique run-in period. We attribute the enhanced lubricity, with steady coefficient of friction <0.05 at 1 N load, to the formation of a transfer layer which incorporates GSs, NDs and nanoscroll structures self-assembled during sliding. High-resolution electron microscopy and Raman spectroscopy indicate that NDs, besides enabling the erosion of the highest interfacial micro-asperities, do assist the transfer layer development via GSs milling. Our findings contribute to the current quest for superlubricity in realistic tribo-contacts meeting industrial standards.

1. Introduction

Diamond-like carbon (DLC) coatings are widely used in various industrial contexts for their protective, antiwear and self-lubricant properties, and recently they found application in biomedical and food industries due to their biocompatibility and suitability for direct contact with food [1–7]. To date, their most extensive use is in the mechanical engineering industry [4,8,9]. As an amorphous material, DLC properties are not univocal but strongly depend on several variables - including the deposition parameters - that ultimately impact the sp^2/sp^3 hybridization ratio. Young's modulus and hardness are not only affected by the carbon hybridization state, but also by the hydrogen content and by the presence of dopants. In general, a remarkably low Coefficient of Friction ($CoF \leq 0.1$) was reported for hydrogenated DLC (H content above 35 %) in vacuum or inert-gas atmosphere. On the contrary the CoF is usually higher in air, signaling that the hydrogen content is not the only key factor [10]. The excellent DLC lubricity has been attributed to graphitization phenomena at the contact interface. These are usually hindered when sliding in air, in favor of interfacial tribochemical reactions driven by ambient oxygen and moisture [11–13]. Nonetheless, metal-DLC contacts are among the most investigated solutions to replace bare metal-metal contacts in ambient air, as coating metals by DLC is a relatively accessible and low-cost technology on an industrial scale. The diffusion of this coating technology further motivates the effort to

* Corresponding authors.
E-mail addresses: renato.buzio@spin.cnr.it (R. Buzio), guido.paolicelli@nano.cnr.it (G. Paolicelli).

https://doi.org/10.1016/j.diamond.2024.111149
Received 26 February 2024; Received in revised form 8 April 2024; Accepted 29 April 2024
Available online 1 May 2024

enhance the DLC tribological response through novel functionalization schemes.

Several studies have shown that the DLC performance benefits of surface functionalization with other solid lubricants or two-dimensional (2D) materials, such as carbon nanomaterials [14,15], molybdenum disulfide (MoS_2), hexagonal boron nitride (h-BN) and transition metal dichalcogenides. For example, Gu et al. [16] evaluated the tribological behavior of multilayer 2D graphene and 3D graphene foams, deposited by drop-casting on DLC and hydrogenated DLC films. A significant friction reduction in ambient air was found against steel and alumina ball bearings, with similar properties for 2D and 3D functionalization species. The analysis of the contact region indicated the formation of a uniform Transfer Layer (TL) with sp^2 hybrid structures induced by 2D or 3D graphene composites. Qi et al. [17] recently proposed a similar strategy to achieve low friction and wear between an amorphous carbon coating and a metallic counterpart, in fact exploiting the synergy of 3D graphene and h-BN. Here, the improved tribological behavior in air reflects the formation of an ordered and compressed TL at the sliding interface that successfully prevents direct contact between metal surfaces. Wang et al. [18] achieved ultra-low friction at high load in ambient air on hydrogenated amorphous carbon film, by sliding spherical steel balls against steel surfaces both covered with sp^2-rich structures (i.e. fullerene-like carbon) or nanocrystalline planar graphitic moieties (i.e. graphitic-like carbon). Such a behavior was attributed to different re-hybridation pathways induced by sliding and by the initial coating properties. The aforementioned examples refer to situations in which functionalization favors the generation of a graphitic TL at the metal-DLC contact, or better, it strongly enhances the sp^2 character of this layer. However, a different functionalization scheme has been recently introduced involving both planar nanostructures with self-lubricating characteristics (graphene [19–22], MoS_2 [23,24]) and hard nanoparticles (nanodiamonds). These nanostructures work in synergy and promise to achieve ultra-low friction behavior (CoF < 0.05).

In fact, Berman et al. [25] obtained ultra-low friction in an inert-gas atmosphere by sliding a DLC-coated ball against a silicon substrate previously functionalized with graphene sheets (GSs) and nanodiamonds (NDs). This result was ascribed to the formation of a particular nanostructure named nanoscroll. Nanoscrolls consist of layered graphene structures rolled into a papyrus-like form morphologically similar to multi-walled carbon nanotubes, with the exception of open extremities and side, that wrap around a small, rigid and generally amorphous core, giving rise to a core-shell heterostructure. The proposed nanoscroll formation mechanism includes an initial stage in which reactive graphene sheets interact with the dangling bonds on the nanodiamonds surface starting the core-shell particles formation, followed by a rolling process forming an outer shell of variable thickness. The ultra-low friction was thus attributed to the reduction in the interfacial contact area, in view of the presence of the nanoscrolls and of their crystalline incommensurability with the DLC surface. Moreover, Berman et al. [25] identified moisture as the main responsible for the friction increase in ambient conditions, since it enhances the graphene-substrate adhesion and prevents the scroll formation with subsequent hard core caging. Later it was hypothesized that the nanoscrolls could form also without direct DLC functionalization [26–28]. Finally, nanoscroll structures have been obtained through encapsulation of various metal nanoparticles [29,30]. We note that, although research work on this topic has been intense in recent years, friction experiments have mainly targeted nanorough DLC layers grown by laboratory deposition facilities over ultra flat substrates (typically Si wafers). Moreover just a few studies addressed the metal-DLC contact, which certainly represents one of the most important systems for the mechanical industry.

In this study, we evaluate the tribological performance of an industrial DLC coating, functionalized with GSs and NDs, sliding against a steel ball bearing. The DLC coating consists of a micrometer-thick film, deposited through plasma-assisted chemical vapor deposition (PA-CVD) on top of a ceramic multilayer structure tailored to improve the overall hardness and corrosion resistance. Notably, the DLC surface morphology displays a double-scale roughness, one located on the micrometer length scale and associated to the cauliflower-like structure of the ceramic interlayers, and a second one on the nanometer level inherent to the DLC film. The tribological tests show a substantial improvement of the lubricity of functionalized DLC with respect to pristine DLC, with CoF approaching 0.05 in dry atmosphere. On the contrary, friction tests conducted on DLC functionalized respectively by GSs, or by NDs, led to a higher CoF value, hence confirming that the functionalization efficacy needs the synergistic use of both allotropic forms. Analysis of sliding tracks on the functionalized DLC substrate attests a wear process localized at the highest protrusions associated to the micrometer scale roughness, while on the steel countersurface the contact region corresponds to a quasi-circular wear scar coated by an irregular carbonaceous TL. A detailed Raman Spectroscopy analysis indicates the TL to be composed of DLC residues, namely a-C, and NDs, isolated and/or wrapped in GSs patches. These results appear promising in engineering contexts, particularly to functionalize the tribological performances of industrial components.

2. Materials and methods

2.1. Substrate and DLC coating

The DLC coatings used in this study were realized upon our request by STS Group s.r.l. (Italy). The coatings were deposited on a flat-faced disc-shaped metal substrate (diameter 45 mm), i.e. a standard configuration suitable for laboratory tribological measurements, via industrial processes according to a specific multilayer architecture. The substrate consists of aluminum alloy (AlSi10Mg) metallic disks whose surface undergoes a mechanical grinding finishing process before deposition. Between metallic substrate and DLC film, different functional layers were grown, respectively: an electroless Nickel-phosphorus plating (thickness 25 μm) to improve mechanical properties such as hardness and the resistance to corrosion, a Cr/CrN interlayer to optimize the DLC coating adhesion to the substrate and a WC/C layer composed of tungsten carbide lamellae alternate to amorphous carbon lamellae, which provides the better matching between substrate and coating (overall thickness 1.2 μm). The DLC coating was finally deposited through PA-CVD at a temperature of 250 °C obtaining an amorphous hydrogenated carbon coating (a-C:H) with a mixture of sp^2 and sp^3 hybridizations of carbon atoms and a typical thickness of 1.5 μm. The DLC surface, characterized through a contact profilometer (KLA Tencor, P-6 Stylus Profiler, tip radius of 2 μm and 60° cone angle) reveals a mean square roughness of Sq = (0.47 ± 0.05) μm.

2.2. Graphene and nanodiamonds deposition

Before functionalizing the disc-shaped DLC substrate, the surface was cleaned with isopropanol in an ultrasonic bath and exposed to plasma oxygen, with a plasma cleaner, to make the surface hydrophilic. Such a treatment facilitates the graphene deposition, allowing the spreading of the colloidal solution containing graphene flakes, which otherwise would remain confined to a small portion of the DLC substrate. As a first step of functionalization, the graphene flakes were deposited using a commercial solution in Ethyl Alcohol (Graphene Supermarket by Graphene Laboratories Inc., Calverton NY) having a final graphene concentration of 1 mg/L. The solution contains mostly single-layer graphene flakes with an estimated size within the range of 0.5–2 μm suspended in ethanol [31]. The surface coverage was achieved by the following procedure. Briefly, a small amount of the suspension, precisely 15 drops, for a final amount of ~1 mL, was consecutively deposited on DLC substrate in a colloidal liquid state, letting Ethyl Alcohol evaporate after each drop deposition thanks to a slight nitrogen flow. Such a procedure resulted in a non-uniform coverage of the sample, including regions where few-layers flakes (3–4 layers) were overlapped, regions

covered by single-layer graphene and areas where DLC surface remained uncovered. Indeed, the inhomogeneity of graphene deposited from the liquid phase is a common feature already reported in other studies, involving different graphene sources, deposition methods and supporting substrates [32,33]. As the second step of the DLC functionalization, detonation nanodiamonds (NDs) with a particle size of 4–6 nm (type: uDiamond®Molto, purchased from Carbodeon Ltd. and used as received) were deposited on the DLC substrates previously functionalized with graphene flakes. Before the deposition, the NDs stored in isopropanol suspension, were sonicated to break up large agglomerates spontaneously formed in the stationery suspension. NDs exhibit a very high content of sp^3 hybridized carbon atoms (>99 %) resulting thus in nanoparticles with a hardness and Young modulus similar to diamond but delivered to the nanoscale. A small amount, precisely 6 drops of volume 70 μL of NDs in isopropanol solution (1 mg/mL) was deposited on the substrates of interest resulting in 0.420 mg of NDs per 15 cm^2. The samples were then dried under nitrogen flow promoting both NDs dispersion and isopropanol evaporation.

2.3. Experimental techniques

2.3.1. Raman spectroscopy

The Raman spectra were acquired with an apparatus working at 532 nm wavelength (LabRAM HR Evolution - Horiba, Jasco NRS-4100 Laser Raman Spectrometer). To avoid surface damages the total power reaching the sample has been adjusted between 1 and 5 mW. Furthermore, the Raman spectra were acquired using an objective with magnification 100× and 600 g/mm diffraction grating. These accurate procedures ensure no visible damage on the surface and no change of spectral shape during the measurements. The data were acquired in the range between 500 and 3500 cm^{-1}.

2.3.2. Ball-on-disc tribometer

Tribological tests were performed using a CSM ball-on disk tribometer. The instrument was composed of a rotatable sample holder, where the sample disk was fixed and of an upper arm, where a dead mass corresponding to the external load was applied. The counterpart was a steel 100Cr6 sphere with a diameter of 4 mm, to simulate a typical industrially relevant tribological contact between DLC and stainless steel. The system was positioned in a sealed chamber, equipped with venting orifice and a gas line enabling a constant gas flow of nitrogen (i.e. N_2). Measurements were conducted at constant linear velocity (10 mm/s) with a typical duration of 1800 s. Different tests were conducted on the same sample simply by changing the contact position on the disc (track radius). The applied load was fixed to 1 N, producing a maximum Hertzian contact pressure of about 0.8 GPa. The condition of contact with zero applied load was obtained through a system of counterweights before the application of the desired load for the experiment. The zeroing procedure for the load was applied to every single measurement. The chamber was equipped with a thermometer and a hygrometer, to monitor the ambient conditions during the tests. Each test was repeated in two different sliding conditions: the HUMID AIR condition, corresponding to sliding in ambient air at a relative humidity between 50 % and 60 %, and the DRY N_2 condition, characterized by a relative humidity of 15 % and by reduced atmospheric oxygen. The latter condition was obtained by flowing high purity N_2 inside the chamber. During the tribological tests, all the parameters of the measurements were kept constant to have reproducible and comparable results.

2.3.3. Atomic Force Microscopy (AFM)

An ambient pressure NTEGRA AURA NT-MDT AFM microscope was used to investigate the topography of the DLC coating, before and after the functionalization. The AFM images were acquired in semi-contact (tapping) mode in air, under ambient conditions, using rectangular-shaped silicon cantilevers (MikroMasch HQ: CSC37/NoAl) with nominal elastic constants between 0.2 and 0.8 N m^{-1} and a resonance frequency between 20 and 40 KHz. Imaging analysis was performed by using the free software Gwyddion (v. 2.41).

2.3.4. Scanning Electron Microscopy (SEM) and Energy Dispersive Spectroscopy (EDS) analysis

The morphological characterization of the functionalized coating after the tribological test was performed using the Leica Cambridge S360 Scanning Electron Microscope, equipped with an Energy-Dispersive Spectrometer (EDS) Oxford X-Max 20 for semi-quantitative compositional analysis and elemental mapping. Additionally, we accomplished high-resolution SEM imaging of worn surfaces and of focused ion beam (FIB)-milled cross sections using the CrossBeam 1540 XB by Zeiss.

2.3.5. Optical microscopy and removed volume analysis

The wear scars on the steel balls were characterized in terms of removed volume V_{ball}, calculated using top-view optical microscopy images (Olympus BX51M, 10╳ magnification). All the wear scars were approximated by a circular area $A = \pi r^2$ and the ball worn volume was assumed equal to a spherical cap of base A and height h. The cap height and the removed volume were derived from the area of the circular wear scar A as $h = R\text{-}(R^2\text{-}r^2)^{1/2}$ and $V_{ball} = \pi h^2(R - h/3)$, where $R = 2$ mm and $r = (A/\pi)^{1/2}$.

3. Results and discussions

3.1. DLC film characterization

The multilayer scheme representative of the coating used in this study is shown in Fig. 1a. The final DLC layer was analyzed using several characterization techniques including Raman spectroscopy, AFM and SEM. Since a visible laser excitation source (532 nm) was used for Raman analysis, then spectra are directly sensitive only to sp^2

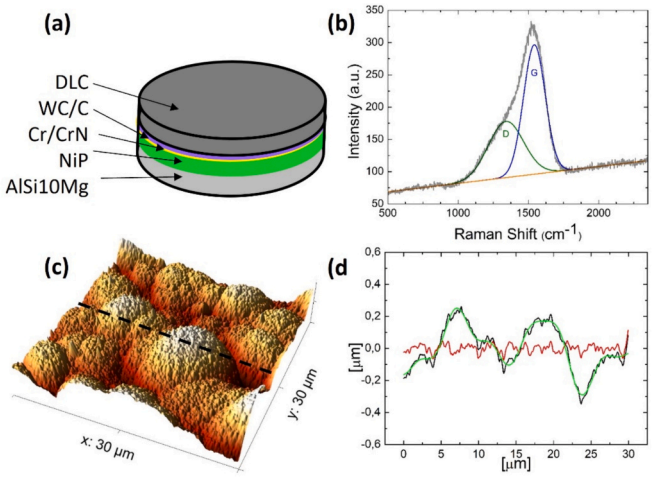

Fig. 1. Multilayered DLC-coated disc used in this study. (a) Not-to-scale schematic diagram of the disc including the metal substrate AlSi10Mg (light gray), the electroless Nickel-phosphorus plating (green), the Cr/CrN interlayer (yellow), the WC/C layer (purple) and the DLC coating (gray). (b) Raman spectrum of pristine DLC coating: raw data (gray line), deconvolution of D and G peaks (respectively, green and blue lines) and baseline (orange line). The following parameters were derived from the fitting analysis, averaged over several spectra acquired in different positions on the sample: D peak (Position: 1357 ± 17 cm^{-1}; Full Width at Half Maximum: 320 ± 30 cm^{-1}; Intensity: 95 ± 7 a.u.). G peak (Position 1543.5: ±1.2 cm^{-1}; Full Width at Half Maximum: 176 ± 6 cm^{-1}; Intensity: 195 ± 6 a.u.). Baseline slope: 0.0262 ± 0.0001. (c) 3-D morphology reconstruction from a representative AFM image of the pristine DLC film (lateral size: 30 × 30 μm^2); (d) topographic profiles along the black dashed line in (c): texture morphology (black line), long-scale roughness (green line) and short-scale roughness (red line). The latter is obtained by subtracting the long-scale roughness profile from the texture.

hybridized bonds [34]. Indication about the relative content of bonded hydrogen (C—H) and the sp^2/sp^3 ratio has been indirectly obtained through a detailed analysis of the Raman signals. The typical Raman spectrum of pristine DLC in the region between 500 and 2500 cm^{-1}, where D and G peaks corresponding to sp^2 vibrational mode are visible, is reported in Fig. 1b. A fitting procedure consisting of a linear background subtraction and a double Gaussian peak fit was used to extract parameters corresponding to the single D and G components as well as the slope of the linear background (Fig. 1b, caption). Starting from these parameters and following the phenomenological approach introduced by Casiraghi et al. [35], the hydrogen percentage of the DLC coating was found to be H% = 24 ± 8 while the sp^3 content within the DLC coating was estimated to be about 40 %. These characteristics are compatible with the hardness parameter H guaranteed by the manufacturer (~21 GPa).

The DLC morphology was investigated by AFM (Fig. 1c); the three-dimensional 3D AFM reconstruction indicates the coating compactness with grains of lateral size below one micron that coalesce to form larger globular structures separated by very compact boundaries. Such a cauliflower structure, typical of the Ni—P interlayer [36,37], is replicated by the Cr/CrN and WC/C interlayers as well as by the final DLC coating, this being a sign of their excellent adhesion to the Ni—P interlayer. A detailed analysis of the DLC morphology reveals the presence of small-range corrugations superimposed on the globular agglomerates. We deconvoluted the morphology profile into two components (see Supporting Information and Fig. SI_14 for details) with the aim to identify two characteristic length scales for the surface roughness (Fig. 1d); a 'long-scale roughness' in the micrometric range ascribable to the Ni—P interlayer coating (Rq: 0.55 ± 0.04 μm in agreement with to the one measured by the profilometer, Sq: 0.47 ± 0.05 μm) and a 'short-scale roughness' in the tens-of-nanometers range, which is intrinsically related to DLC (Rq: 27.2 ± 5 nm).

DLC coatings were then functionalized using a combination of graphene sheets (GSs) and NDs. The functionalization procedure we used was firstly applied by Berman et al. [25] and it has been deeply exploited over the last decades to enhance the tribological performances of several contact junctions, both carbonaceous and not [38–42]. It consists in the sequential deposition of graphene flakes followed by a subsequent deposition of NDs, both dispersed in liquid solutions (Fig. 2a, b). A qualitative estimation of the graphene deposited on DLC was performed by AFM. Height and phase signals, shown in Fig. 2c, d, revealed the presence of tiny structures reasonably ascribable to the presence of graphene. In particular, while the height signal (Fig. 2c) reveals only the presence of large agglomerates together with the typical wrinkles and ripples, intrinsically related to the out-of-plane deformation of graphene (highlighted by green arrows), the phase signal shows a clear contrast across graphene flakes placed on the DLC structures. On phase image (Fig. 2d) it is possible to discriminate at least three different regions: the DLC substrate (darker regions), graphene sheets spread out – even multilayered - (brighter regions) and balled up and crumpled graphene flakes (white spherical agglomerates) and this morphology was confirmed by Raman analysis (for a detailed discussion of the Raman signal related to each functionalization step, see Supporting Information, Figs. SI_1-SI_7).

Fig. 2e shows a SEM image of DLC functionalized with GSs and NDs where it is possible to distinguish the globular DLC structure as well as the NDs aggregates of different size; some of them tend to agglomerate forming NDs clusters, others are fairly dispersed. The image confirms a very high NDs coverage degree so that the portion of the DLC surface not covered by NDs is really small; GSs are not visible because of poor contrast with respect to the DLC substrate and they are probably widely covered by the thick layer of NDs. Raman analysis was performed on the multi-functionalized surface. However, despite the deposition being intrinsically non-uniform, the Raman signal does not show any particular variability without highlighting either the presence of GSs or NDs. The only visible structures are those of the DLC and the spectrum is very similar to the one already shown in Fig. 1b (more details in Supporting Information, Fig. SI_6 and SI_7).

3.2. Friction analysis

The tribological behavior of functionalized DLC was then investigated both in humid air and in dry N_2 conditions with the tribometer working in ball-on disk configuration, using circular unidirectional sliding and a steel 100Cr6 sphere with a diameter of 4 mm as counterpart (Fig. 3a). Fig. 3b shows the CoF vs sliding cycles trend for the system functionalized with both GSs and NDs. The test in humid air starts with a run-in, characterized by a CoF similar to the one of pristine DLC

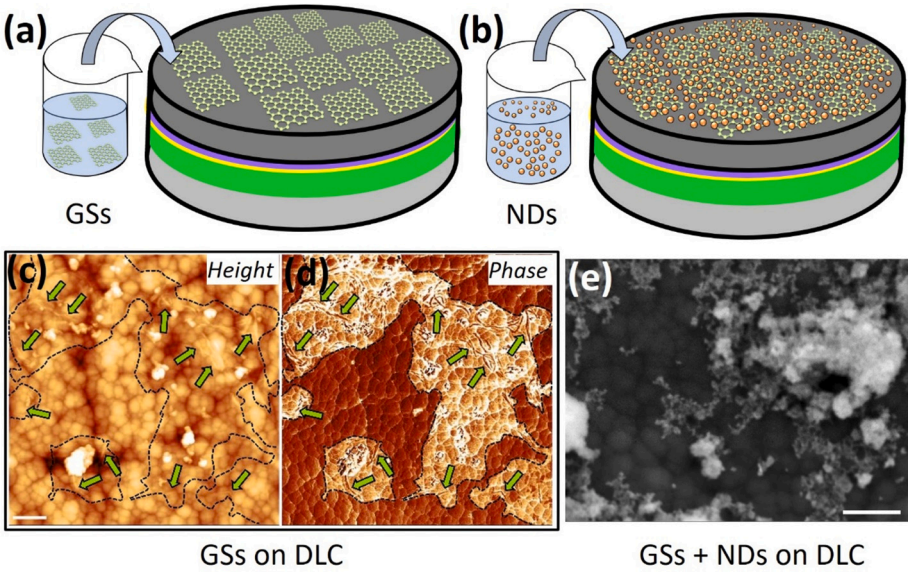

Fig. 2. DLC functionalization. (a) Not-to-scale schematic of first treatment with graphene sheets (GSs); (b) not-to-scale schematic of second treatment with nanodiamonds (NDs) on previously GSs-functionalized DLC. AFM images of GSs deposited on DLC (c) height and (d) phase signal. GSs borders were identified by phase image then transferred to the height image; typical graphene wrinkles visible in both signals are highlighted by the green arrows (scale bar 1 μm). (e) SEM image of GSs-NDs functionalized DLC showing NDs inhomogeneous coverage and clustering over the DLC cauliflower-like structure (scale bar 1 μm).

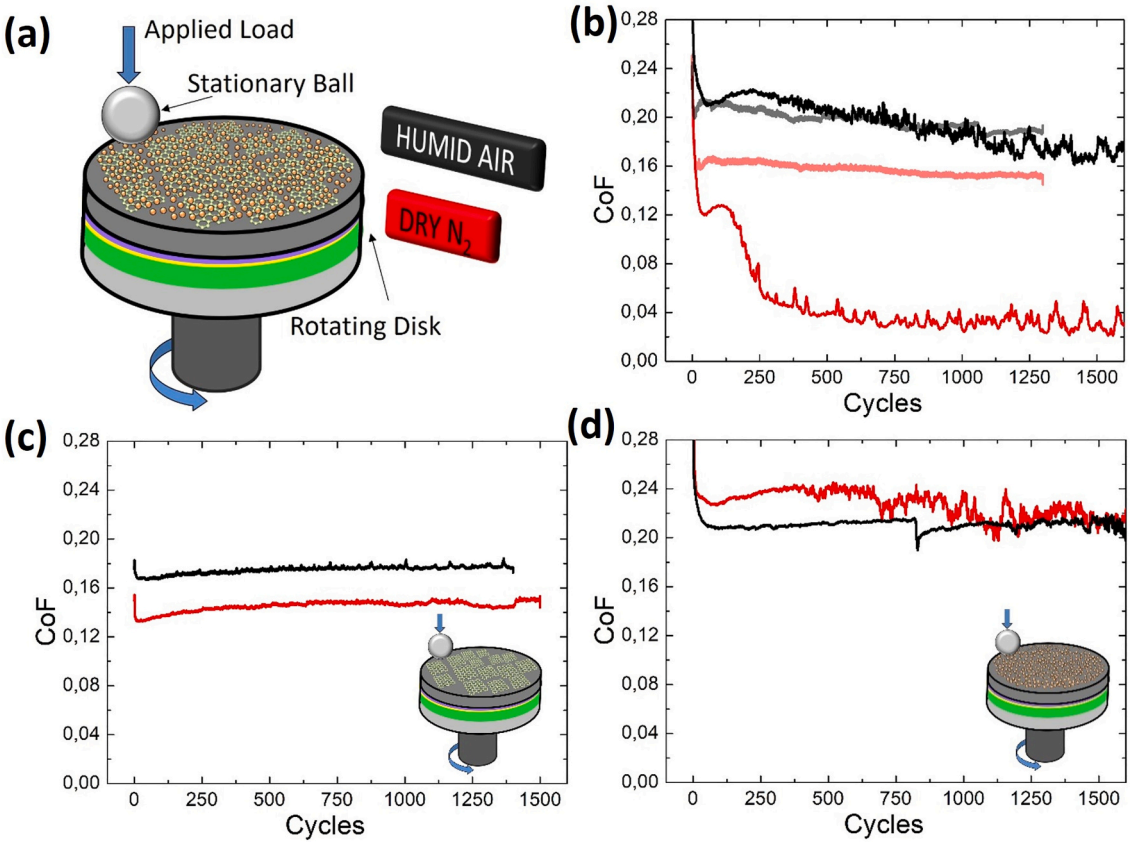

Fig. 3. Steel vs functionalized DLC tribological behavior at 1 N load and 10 mm/s constant linear velocity. (a) Not-to-scale schematic of the tribological test. (b) CoF plots of GSs-NDs functionalized DLC in humid air atmosphere (black lines) and in dry nitrogen (red lines); shadowed lines correspond to pristine DLC in humid air and dry nitrogen atmospheres, respectively. (c) CoF plots of GSs-functionalized DLC in humid air atmosphere (black lines) and in dry nitrogen (red lines); (d) CoF plots of NDs-functionalized DLC in humid air atmosphere (black lines) and in dry nitrogen (red lines).

(shadowed line). After this transition, the CoF decreases, the signal becomes noisier and finally achieves a value slightly lower with respect to pristine DLC. On the contrary, the CoF in a dry N_2 atmosphere decreases immediately with respect to the pristine and, after a run-in period, it reaches a remarkably low and steady value of <0.05. This ultra-low friction steady state appears noisy, but CoF values never exceed 0.075. Measurements in a dry N_2 atmosphere have been repeated on different positions and different samples to assess the robustness of the functionalization strategy (see Supporting Information, Fig. SI_13a). In all the analyzed situations a steady state was reached and the CoF reduction was evident. The average CoF value obtained from the ensemble of these measurements is 0.07 ± 0.03. Finally, an endurance test lasting about 4 times the standard ones has further confirmed the validity of this procedure (Fig. SI_13b).

The synergistic effect due to the presence of GSs and NDs was verified through two different control measurements. Results concerning the DLC substrate functionalized with only GSs are presented in Fig. 3c. The presence of graphene flakes slightly improves the slip properties both in humid air and in dry N_2 atmosphere but only in the initial phase. The run-in period is practically eliminated but the CoF increases with the sliding cycles approaching values characteristic of pristine DLC. This behavior seems in agreement with the classic model that explains the lubricating effect of DLC as due to the creation of a graphite-type film at the interface during the first moments of sliding [11,13,27,43–46]. The presence of graphene already distributed on the contact surface drastically reduces the time of formation of the sliding graphitic layer but it does not affect the long-term CoF behavior signaling that no particular characteristics in the growth and composition of the transfer layer are present in this case. Tribological tests were performed as well on DLC functionalized with only NDs powder. Fig. 3d shows a clear worsening of the CoF with respect the case of pristine DLC, both in humid air and in a dry N_2 atmosphere (CoF $\sim$ 0.22), revealing a scraping behavior typical of small and hard materials such as NDs which, alone, act like an abrasive tool.

The combination of all these tribological tests highlights the effects of the functionalization revealing the simultaneous presence of both carbon allotropes, GSs and NDs, as an essential condition for improving the friction response at the macroscale level. The tribological results and, in particular, the absence of a strong CoF reduction in ambient air on GSs-NDs DLC, suggest that the mechanism hypothesized by Berman et al. [25] for improving friction through nanoscroll formation can also act in this system. According to the model in fact, the sliding should induce GSs to wrap around the NDs forming nanoscroll and promoting lower surface contact, but the nanoscroll structures are stabilized by van der Waals forces only in the absence of water molecules in the contact region. In the absence of NDs, the GSs does not self-wrap or if the wrapping happens the created structures are not sufficiently resistant to the locally applied load.

3.3. Disk tracks analysis

After tribological tests on the functionalized DLC substrate, the sliding tracks are recognizable but they do not show any measurable wear from profilometer measurements. In order to decipher the underlying origins of low friction behavior, all the tribological tracks as well as the ball contact regions were analyzed by SEM and Raman spectroscopy both on the pristine DLC and the functionalized DLC samples. Fig. 4a shows a SEM image of the track obtained on pristine DLC in dry N_2

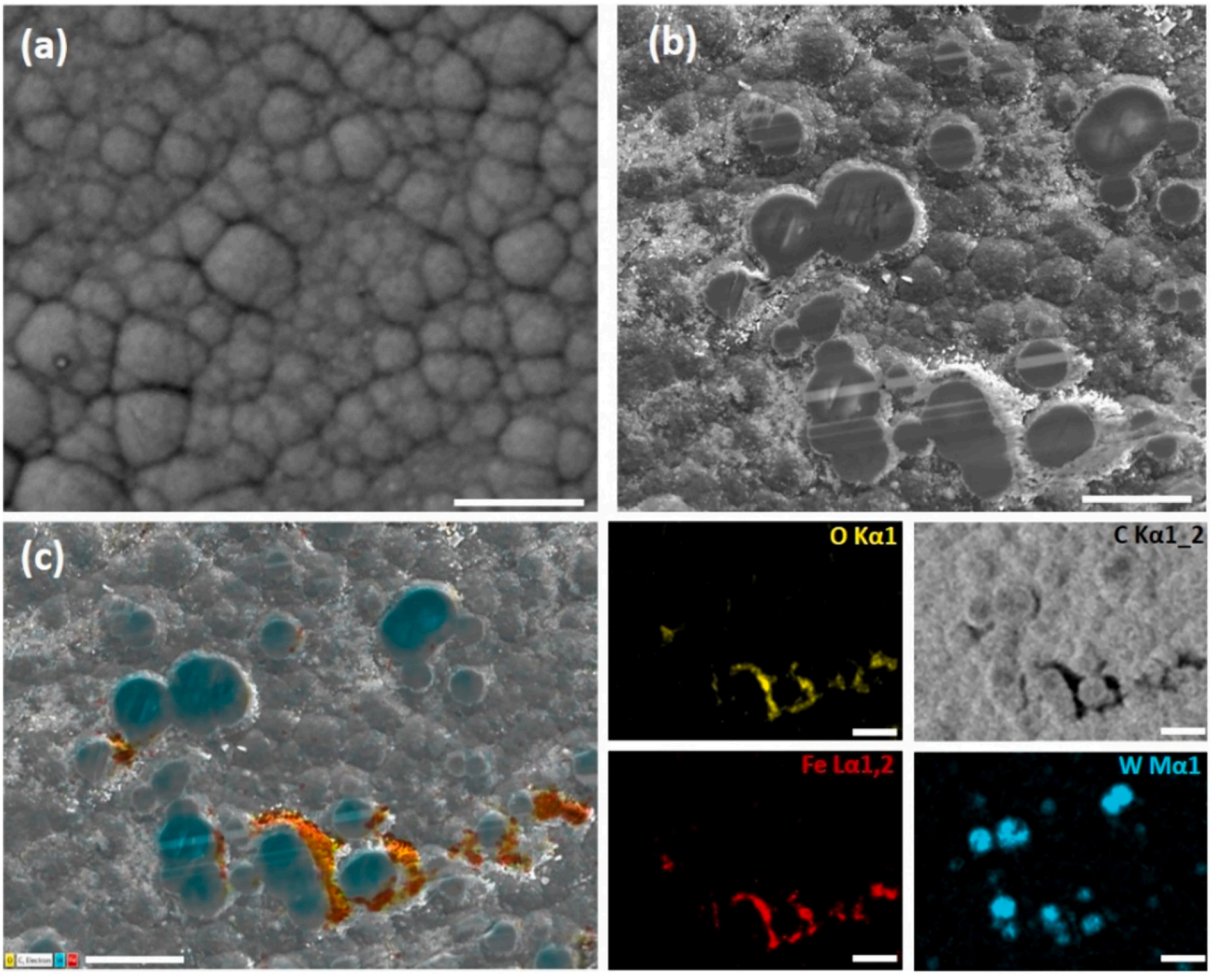

Fig. 4. SEM/EDS micrographs of the DLC track (a) Pristine DLC and (b) GSs - NDs functionalized DLC within a sliding track (normal load 1 N; dry N_2). (c) EDS analysis of the functionalized DLC region in (b): layered image and elemental map of O (yellow), C (gray), Fe (red) and W (cyan). Scale bars: 20 μm.

atmosphere revealing the typical globular structures (associated to the long-scale roughness) perfectly unaltered, namely very similar to the original morphology before the sliding. Interestingly, the SEM images of the tracks on functionalized DLC reveal a partial wear process on the DLC coating, in particular on the top of highest agglomerates/bumps, which appear truncated as shown in Fig. 4b. In addition to the flattening of the DLC protrusions, SEM analysis shows accumulation of material from the ball alongside the flattened areas. The EDS mapping highlights both the wear of the DLC - resulting in the enhancement of the tungsten signal from the WC/C layer underneath - and the wear of the ball – as deduced from the localization of iron (Fe) and oxygen (O) signals on the sides of the worn protrusions (Fig. 4c).

The sliding tracks on pristine and functionalized DLC have been examined also by Raman spectroscopy. Spectra collected on the pristine DLC sample inside the track are reported in the Supporting Information (Fig. SI_8a), and they reveal only the characteristic D and G structures of the DLC surface. On the contrary, spectra collected on the functionalized DLC surface inside the track corresponding to Fig. 4b (i.e. dry N_2 atmosphere) exhibit a dual behavior (Fig. 5a). There are regions where the Raman signal clearly corresponds to the already observed DLC features, and regions in which sp^2 related peaks appear. DLC-like spectra were modeled with two components corresponding to D and G bands whose position and width are comparable to those found on pristine DLC as well as on the functionalized surface outside the tracks. In the other regions two more components, likely corresponding to sp^2 related features, have to be introduced (Fig. 5b and Table I). These graphitic signals appear with variable intensities creating spectra where both the DLC-related D and G peaks and the sp^2 features are recognizable, but also spectra in which the sp^2 features completely overcome other signals. These results appear in perfect agreement with the high-resolution SEM images of the wear tracks (Fig. 5c and d). Inside the tracks few layer graphene flakes randomly distributed on top of the DLC globular surface as well as agglomerates of NDs are clearly visible. The former gives rise to the intense sp^2 Raman signal while, the latter, are not detectable because of low sensitivity of visible excitation to sp^3 bonds.

3.4. Ball counterface analysis and friction mechanisms

The erosion occurring on the steel balls was the most evident and quantifiable wear effect (Fig. 6a). The wear scars at the end of the tribological tests - conducted in four different situations as those presented in Fig. 3b - were carefully evaluated and the removed volumes V_{ball} are reported in Table II.

According to Table II, the steel balls sliding on functionalized DLC suffer significantly less wear compared to the pristine DLC substrate case, regardless of the working environment. The effect could be readily connected to the growth of a specific and highly protective TL on the steel ball that prevents direct contact between the DLC substrate and the steel counterface. V_{ball} achieves a minimum in dry N_2 atmosphere, and this value is almost equal to that removed during the initial run-in phase, hence we conclude that under the most lubricious conditions the TL grows up during the run-in, and then it remains stable.

We corroborate such findings through a refined investigation of the wear scar under dry N_2 sliding conditions. A large-scale SEM analysis of

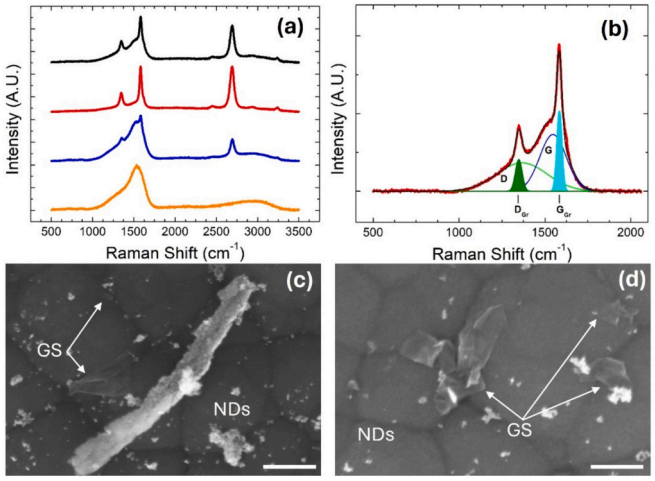

Fig. 5. Raman spectra and high-resolution SEM images collected inside the wear tracks on functionalized DLC after sliding test on dry N_2 atmosphere. a) Representative Raman spectra on different locations b) deconvolution of DLC-like and graphene-like peaks on Raman spectra corresponding to black curve on panel (a). Spectra are modeled with four components corresponding to D and G bands from the DLC surface and D_{Gr} and G_{Gr} peaks of graphene. c) and d) Representative high resolution SEM images showing respectively: isolated GSs having a lateral size much smaller than the nominal one declared for the liquid solution; linear nanoscroll-like nanostructures; NDs agglomerates. Scale bars: 200 nm.

the ball surface slid against functionalized DLC reveals the formation of a circular wear scar surrounded by loose debris particles (Fig. 6a). EDS elemental analysis conducted at a similar magnification indicates that the debris is mainly composed of carbonaceous species while, on the wear scar, the spectrum is dominated by the iron signal (Fig. 6b).

Given the dry N_2 sliding conditions, there is no relevant increase of the oxygen signal (compared to the unworn steel surface) that might indicate tribo-induced oxides formation within the contact region. Both high-resolution SEM and Raman measurements (Figs. 7, 8) attest that a thin carbon-based TL indeed covers this region. A detailed morphological analysis of the circular worn contact region is presented on Fig. 7. Within the contact area, the TL clearly appears as a patched distribution of sub-micrometric deposits arranged into sliding-induced surface striations (Fig. 7a-c). These deposits are much thinner than those located at the periphery of the wear scar, as highlighted by the light-dark contrast in the SEM image. There, the TL appears both as a ~100 nm-thick compact layer, marking the potential trailing edge (Fig. 7d), or as a thicker deposit (>500 nm) located at the leading edge and at the surrounding areas (Fig. 7e). Moreover, the EDS oxygen signal indicates the occurrence of oxidative processes at the contact periphery (Fig. 6b), activated by residual oxygen-related species from the environment. We ascribe the origin of the ultralow COF of functionalized DLC to the peculiar nature of the TL within the contact region. This forms during the run-in (see discussion above and Table II), through a process that in turn reflects the competition between interfacial erosion and the development of a transfer film involving DLC, GSs and NDs, until a stable contact is achieved. This description is perfectly coherent with the CoF vs sliding cycles (Fig. 3b) where it is clearly visible a longer run-in period (typically hundreds of cycles) with respect to pristine DLC followed by a sudden and marked CoF reduction reaching a steady state value in 400 cycles. The fact that the COF reduction takes place only with the simultaneous presence of the two carbonaceous nanostructures (i.e. NDs and GSs) makes less relevant the DLC erosion process by NDs in the formation of a lubricious TL, whose origin on the contrary should be

Table I
Average values obtained from the deconvolution procedure of DLC-like and graphene-like spectra shown on Fig. 5b. Peak positions and relative FWHM are expressed in cm^{-1}.

	D	*FWHM*	*G*	*FWHM*	D_{Gr}	*FWHM*	G_{Gr}	*FWHM*	$2D_{Gr}$	*FWHM*
DLC like spectrum	***1366***	*317*	***1551***	*176*	–	–	–	–	–	–
Graphene like spectrum	***1367***	*344*	***1547***	*181*	***1350***	*46*	***1586***	*34*	***2693***	*55*

	D		*G*		D_{Gr}		G_{Gr}		$2D_{Gr}$	
	Position	*FWHM*	***Position***	*FWHM*	***Position***	*FWHM*	***Position***	*FWHM*	***Position***	*FWHM*
DLC like spectrum	***1366***	*317*	***1551***	*176*	–	–	–	–	–	–
Graphene like spectrum	***1367***	*344*	***1547***	*181*	***1350***	*46*	***1586***	*34*	***2693***	*55*

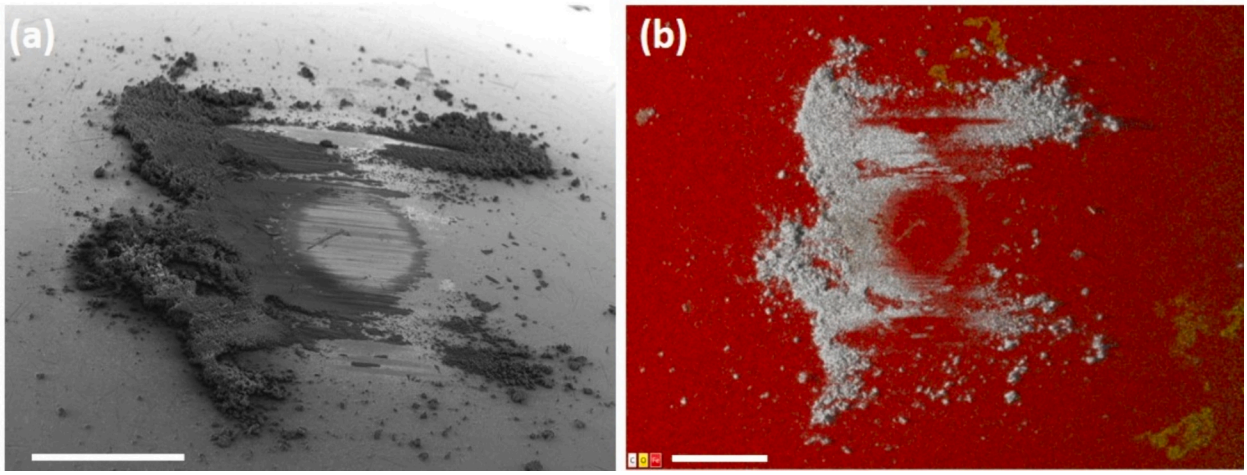

Fig. 6. SEM and EDS micrographs of the steel ball sled against functionalized DLC in dry N_2. (a) Tilted view of the ball contact area showing the TL within and around the circular worn region. (b) EDS-layered top-view image with elemental mapping of O (yellow), C (white) and Fe (red) for the ball region in (a). Scale bars: 200 μm.

Table II
Removed volumes of the steel balls, at the end of tribological tests carried out according to four different situations. In the last row, V_{ball} corresponds to a shorter test intentionally stopped at the end of the run-in phase.

	V_{ball} (mm^3)
DLC Pristine – HUMID AIR	$(3,4 \pm 0,2) \times 10^{-5}$
DLC Pristine – DRY N_2	$(3,0 \pm 0,2) \times 10^{-5}$
DLC Functionalized – HUMID AIR	$(2,2 \pm 0,2) \times 10^{-5}$
DLC Functionalized – DRY N_2	$(2,0 \pm 0,2) \times 10^{-5}$
DLC Functionalized – DRY N_2 Run-in Test. 400 Cycles	$(1,9 \pm 0.2) \times 10^{-5}$

related to the GSs milling by NDs. In this respect, an in-depth SEM analysis of the debris particles on the DLC wear tracks points out the presence of isolated GSs moieties with a lateral size (<100 nm) much smaller than the expected nominal one in the liquid solution (Fig. 5d). This evidence, together with the small number of GSs we observed within the sliding tracks, supports the claim of GSs milling by NDs and incorporation into the lubricious TL distributed over the contact region.

To gain deeper insight into the TL properties, a large campaign of Raman measurements was carried out. Raman measurements were performed randomly within worn contact areas to account for the non-uniformity inherent to the TL growth. A selection of the results is shown in Fig. 8 where a stack of selected spectra obtained on the wear scar after sliding on the functionalized DLC surface, respectively in humid air (Fig. 8a) and in a dry N_2 atmosphere (Fig. 8b), are presented. The bottom panels contain individual spectra that refer to sliding on the pristine DLC. In this last case, traces of carbonaceous species are very weak and poorly structured. On the contrary, the spectra related to the sliding on functionalized DLC show two new structures located in the spectral region between 1000 and 2000 cm^{-1}. Compared with the typical spectrum obtained on pristine DLC (Fig. 1b) these structures are clearly different and indicative of the formation of a specific TL on the surface of the mating steel balls [27].

Moreover, there is a clear difference as a function of the environmental conditions. The ball counterface that worked in dry N_2 presents new, well visible, and sharp structures, while on the counterparts used in humid air such structures appear as weak shoulders on a larger signal and, in some regions, they are practically indistinguishable compared to the underline broad signal. The superimposition of Raman signatures from counterparts who worked in dry N_2 and in humid air atmospheres respectively, are shown in Fig. 8c to mark the different signal intensity depending on the environmental conditions. In any case the new structures appear in the same spectral regions in both systems. In

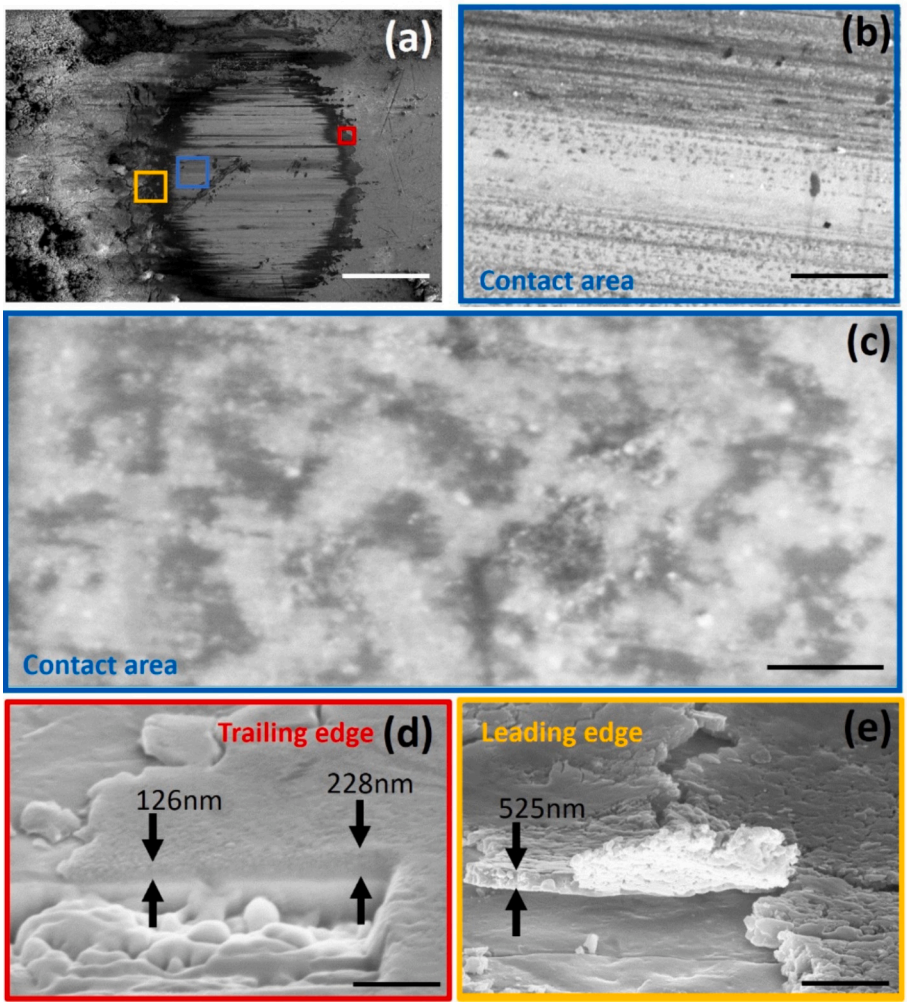

Fig. 7. (a) SEM micrograph of the ball contact area showing the TL within and around the circular worn region. The TL deposits are thinner within the contact region than at the contact periphery, as highlighted by the clear-dark contrast. Scale bar: 75 μm. (b), (c) SEM magnifications of the blue square region in (a), located within the contact area: they show a patched distribution of deposits arranged into sliding-induced surface striations. Scale bars, respectively: 8 μm and 300 nm. (d) SEM magnification of the red square region in (a) at the trailing edge: inspection of the TL cross-section, prepared by FIB milling, allows to estimate the local TL thickness in the range 120 - 230 nm. Scale bar: 430 nm. (e) SEM magnification of the yellow square region in (a) at the leading edge: here the TL consists of micrometric platelets of thickness of about 500 nm. Scale bar: 3 μm. The thickness measured by FIB milling gives a rough upper limit to the TL thickness within the contact area.

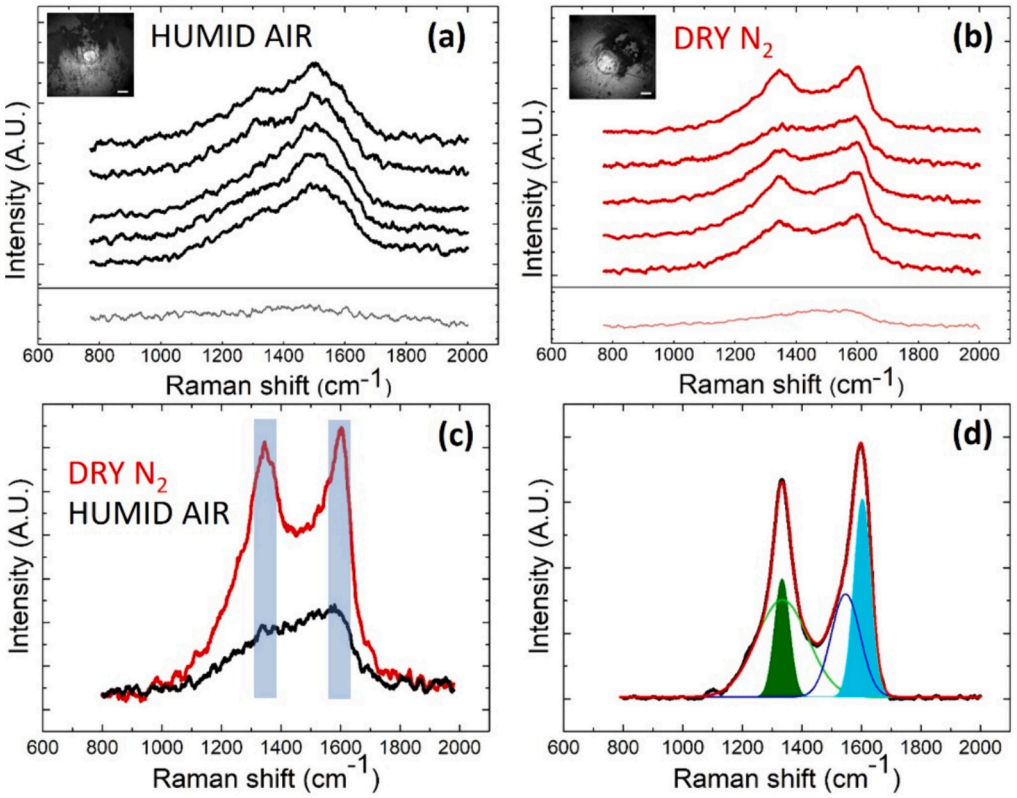

Fig. 8. Raman spectra acquired on the ball contact region slipped on functionalized DLC (a) in humid air and (b) in dry N_2 atmosphere, respectively. The single spectra in the bottom panels refer to the ball contact region slipped on pristine DLC. Insets images refer to the ball contact regions after the sliding; scale bars: 100 μm. (c) Comparison of Raman spectra in dry N_2 (red) and in humid air (black) respectively: the two signatures in the spectral regions highlighted in shaded blue between 1320 and 1350 cm^{-1} and 1590 and 1620 cm^{-1} are strongly inhibited in the humid air atmosphere. (d) Deconvolution of the spectrum in dry N_2 into four distinct components: the light green and blue lines at 1334 cm^{-1} and 1547 cm^{-1} respectively, refer to amorphous carbon components while filled green and cyan curves at 1333 cm^{-1} and 1603 cm^{-1} refer to the characteristic TL involving the NDs contribution.

particular the first one lies between 1320 and 1350 cm^{-1} and the second one between 1590 and 1620 cm^{-1}. This may indicate that the formation of specific nanostructures within the TL is inhibited in humid air compared to the dry N_2 atmosphere. Support to these conclusions comes from background literature [25], as well as from the evidence that in humid air, both the steel surface and the TL reacted with ambient oxygen species (see Supporting Information, Fig. SI_15).

Further insight on the nature of the TL has been obtained by a carefully peak fit analysis of the Raman spectra in dry N_2 atmosphere, an example of which is presented in Fig. 8d. Despite the presence of two relatively narrow peaks, the best fitting procedure requires the use of four distinct components. These components are grouped in two subsets, one linked just to the accumulation of amorphous carbon on the ball counterface and present also in the absence of functionalization (Supporting Information, Fig. SI_11). The other subset corresponds to the formation of a particular TL containing nanodiamonds. Amorphous carbon peaks are represented by the light green and blue lines, centered at 1334 cm^{-1} and 1547 cm^{-1}, while the characteristic TL peaks correspond to the filled green and cyan curves centered at 1333 cm^{-1} and 1603 cm^{-1}. The assignment of these peaks derives from the comparison with recent literature which demonstrates that Raman spectra obtained on NDs or thin films containing NDs are always composed by two main contributions [34,47–50]. The typical contribution due to NDs (sp^3 structures) lies between 1320 and 1340 cm^{-1}, while a variable presence of graphitic layers and or functional groups on the NDs surface provides an ever-present broad peak centered around 1600 cm^{-1} [51]. The relative intensity of sp^3 and sp^2 structures depends on the laser excitation energy but a large experimental evidence demonstrates that even with visible sources both structures are simultaneously observed [52–56].

Therefore, Raman and SEM analysis of the spherical counterpart revealed the presence, within the contact region, of a nanostructured TL identified as a patched distribution of sub-micrometric deposits arranged into sliding-induced surface striations. Raman analysis within the circular worn contact region disclosed the TL structure to be composed by amorphous carbon and NDs, isolated or eventually wrapped in GSs, without any signature of isolated GSs patches; in fact, the typical 2D-band around 2700 cm^{-1} is absent while the characteristic broad peak around 1600 cm^{-1} ascribable to the presence of graphitic shells and/or the nanoscrolls presence is clearly visible. Such a behavior further indicates the possible formation of nanoscrolls which are known to be hindered in humid air. According to current literature [25], nanoscroll structures ultimately assist ultralow sliding friction regimes by promoting a reduction of the contact area and the emergence of incommensurability between the graphitic shell and DLC. These mechanisms appear of broad applicability, as attested by the improved lubricity recently achieved with nanoscrolls formed via shear-induced rearrangements of various metal nanoparticles and GSs [29,30].

4. Conclusions

Despite the good tribological results obtained through the use of DLC coatings in metal-to-metal contacts, several investigations have shown that this behavior can be further improved thanks to the synergistic use of nanostructured materials. In this study we attested a significant improvement of the tribological performance of a microrough steel-DLC tribo-contact, upon functionalization with graphene sheets (GSs) and nanodiamonds (NDs) under dry atmosphere. Friction measurements

revealed the functionalization efficacy exclusively with both nanostructures, in other words adding only GSs or only NDs did not improve the DLC tribological response.

The track analysis on the functionalized DLC coating revealed a partial wear process on the top of the highest protrusions which seems the only effect induced by the high roughness of our realistic contact interface. Indeed, after a relatively short run-in phase in which abrasion occurs, the metal-DLC system enters the ultra-low friction regime without any evidence of performance degradation within the limits of the endurance tests presented in this work.

Analysis on the steel countersurface revealed the formation of an irregular carbonaceous transfer layer (TL): in particular, at the periphery of the contact, the TL looked compact but with variable thickness while within the circular worn contact region, the TL was identified as a patched distribution of sub-micrometric deposits arranged into sliding-induced surface striations. Raman analysis within the worn contact region who worked in a dry atmosphere, highlight the presence of nanoscroll structures, i.e. NDs enveloped in GSs, as well as of amorphous carbon. On the contrary, the presence of nanoscrolls is strongly reduced on the counterparts that worked in air. This leads to the conclusion that the formation and presence of these structures in the contact area is the leading effect to obtain an ultra-low friction regime.

The optimization of this functionalization procedure might open the way to a new class of carbon based self-lubricant and protective coating allowing ultra-low friction behavior to be achieved even in industrial contexts.

CRediT authorship contribution statement

Andrea Mescola: Methodology, Investigation, Data curation, Conceptualization, Writing – original draft, Writing – review & editing. **Alessia Lodi:** Data curation, Investigation. **Federico Zanni:** Data curation, Investigation. **Alberto Rota:** Conceptualization, Methodology. **Andrea Gerbi:** Conceptualization, Investigation. **Cristina Bernini:** Writing – review & editing, Investigation, Data curation. **Marine Schott:** Investigation, Data curation. **Luca Repetto:** Investigation, Data curation. **Adalberto Camisasca:** Writing – review & editing, Conceptualization. **Silvia Giordani:** Writing – review & editing, Conceptualization. **Renato Buzio:** Writing – review & editing, Writing – original draft, Supervision, Project administration, Investigation, Funding acquisition, Data curation, Conceptualization. **Guido Paolicelli:** Writing – review & editing, Writing – original draft, Supervision, Project administration, Investigation, Funding acquisition, Data curation, Conceptualization.

Declaration of competing interest

The authors declare that they have no known competing financial interests or personal relationships that could have appeared to influence the work reported in this paper.

Data availability

Data will be made available on request.

Acknowledgements

This work was carried out in the frame of the project PRIN UTFROM Grant No. 20178PZCB5 founded by the Italian Ministry of University and Research and project ECOSISTER funded under the National Recovery and Resilience Plan (NRRP), Mission 04 Component 2 Investment 1.5 –NextGenerationEU, Call for tender n. 3277 dated 30 December 2021 Award Number: 0001052 dated 23 June 2022.

Appendix A. Supplementary data

Supplementary data to this article can be found online at https://doi.org/10.1016/j.diamond.2024.111149.

References

[1] B.K. Gupta, B. Bhushan, Micromechanical properties of amorphous carbon coatings deposited by different deposition techniques, Thin Solid Films 270 (1995) 391–398, https://doi.org/10.1016/0040-6090(95)06699-3.
[2] C. Donnet, J. Fontaine, T. Le Mogne, M. Belin, C. Héau, J.P. Terrat, F. Vaux, G. Pont, Diamond-like carbon-based functionally gradient coatings for space tribology, Surf. Coat. Technol. 120–121 (1999) 548–554, https://doi.org/10.1016/S0257-8972(99)00432-6.
[3] R. Hauert, An overview on the tribological behavior of diamond-like carbon in technical and medical applications, Tribol. Int. 37 (2004) 991–1003, https://doi.org/10.1016/j.triboint.2004.07.017.
[4] S.D.A. Lawes, M.E. Fitzpatrick, S.V. Hainsworth, Evaluation of the tribological properties of DLC for engine applications, J. Phys. D. Appl. Phys. 40 (2007) 5427–5437, https://doi.org/10.1088/0022-3727/40/18/S03.
[5] D. Bociaga, K. Mitura, Biomedical effect of tissue contact with metallic material used for body piercing modified by DLC coatings, Diam. Relat. Mater. 17 (2008) 1410–1415, https://doi.org/10.1016/j.diamond.2008.02.014.
[6] C. Boxler, W. Augustin, S. Scholl, Fouling of milk components on DLC coated surfaces at pasteurization and UHT temperatures, Food Bioprod. Process. 91 (2013) 336–347, https://doi.org/10.1016/j.fbp.2012.11.012.
[7] E. Salerno, D. Casotti, G. Paolicelli, E. Gualtieri, A. Ballestrazzi, G.C. Gazzadi, G. Bolelli, L. Lusvarghi, S. Valeri, A. Rota, Friction and wear of DLC films deposited on additive manufactured AlSi10Mg: the role of surface finishing, Surf. Coat. Technol. 463 (2023) 129531, https://doi.org/10.1016/j.surfcoat.2023.129531.
[8] S.K. Field, M. Jarratt, D.G. Teer, Tribological properties of graphite-like and diamond-like carbon coatings, Tribol. Int. 37 (2004) 949–956, https://doi.org/10.1016/j.triboint.2004.07.012.
[9] P. Kodali, K.C. Walter, M. Nastasi, Investigation of mechanical and tribological properties of amorphous diamond-like carbon coatings, Tribol. Int. 30 (1997) 591–598, https://doi.org/10.1016/S0301-679X(97)00027-3.
[10] C. Donnet, A. Erdemir (Eds.), Tribology of Diamond-like Carbon Films: Fundamentals and Applications, Springer, New York, 2008. https://link.springer.com/book/10.1007/978-0-387-49891-1.
[11] Y. Liu, A. Erdemir, E.I. Meletis, An investigation of the relationship between graphitization and frictional behavior of DLC coatings, Surf. Coat. Technol. 86–87 (1996) 564–568, https://doi.org/10.1016/S0257-8972(96)03057-5.
[12] A. Erdemir, O. Eryilmaz, Achieving superlubricity in DLC films by controlling bulk, surface, and tribochemistry, Friction 2 (2014) 140–155, https://doi.org/10.1007/s40544-014-0055-1.
[13] Y. Liu, E.I. Meletis, Evidence of graphitization of diamond-like carbon films during sliding wear, J. Mater. Sci. 32 (1997) 3491–3495, https://doi.org/10.1023/A:1018641304944.
[14] J. Bartelmess, S. Giordani, Carbon nano-onions (multi-layer fullerenes): chemistry and applications, Beilstein J. Nanotechnol. 5 (2014) 1980–1998, https://doi.org/10.3762/bjnano.5.207.
[15] A. Camisasca, A. Sacco, R. Brescia, S. Giordani, Boron/nitrogen-codoped carbon nano-onion electrocatalysts for the oxygen reduction reaction, ACS Appl. Nano Mater. 1 (2018) 5763–5773, https://doi.org/10.1021/acsanm.8b01430.
[16] W. Gu, S. Qi, W. He, K. Chu, Z. Lu, G. Zhang, Different tribological behaviors in multilayer 2D graphene and 3D graphene foam modified DLC/H-DLC film in moist air, Tribol. Lett. 70 (2022) 16, https://doi.org/10.1007/s11249-021-01556-1.
[17] S. Qi, W. Gu, Z. Lu, Z. Geng, G. Zhang, Low friction and wear of a-C:H films by lubrication of 3D graphene/hexagonal boron nitride composite in atmospheric environment, J. Mater. Eng. Perform. (2022), https://doi.org/10.1007/s11665-022-07297-z.
[18] Y. Wang, K. Gao, B. Zhang, Q. Wang, J. Zhang, Structure effects of sp2-rich carbon films under super-low friction contact, Carbon 137 (2018) 49–56, https://doi.org/10.1016/j.carbon.2018.05.016.
[19] C. Galiotis, O. Frank, E.N. Koukaras, D. Sfyris, Graphene mechanics: current status and perspectives, Annu. Rev. Chem. Biomol. Eng. 6 (2015) 121–140, https://doi.org/10.1146/annurev-chembioeng-061114-123216.
[20] C. Lee, X. Wei, J.W. Kysar, J. Hone, Measurement of the elastic properties and intrinsic strength of monolayer graphene, Science 321 (2008) 382–385, https://doi.org/10.1126/science.1157996.
[21] A. Mescola, G. Paolicelli, S.P. Ogilvie, R. Guarino, J.G. McHugh, A. Rota, E. Iacob, E. Gnecco, S. Valeri, N.M. Pugno, V. Gadhamshetty, M.M. Rahman, P. Ajayan, A. B. Dalton, M. Tripathi, Graphene confers ultralow friction on nanogear cogs, Small 17 (2021) 2104487, https://doi.org/10.1002/smll.202104487.
[22] A. Mescola, A. Silva, A. Khosravi, A. Vanossi, E. Tosatti, S. Valeri, G. Paolicelli, Anisotropic rheology and friction of suspended graphene, Phys. Rev. Mater. 7 (2023) 054007, https://doi.org/10.1103/PhysRevMaterials.7.054007.
[23] E. Serpini, A. Rota, A. Ballestrazzi, D. Marchetto, E. Gualtieri, S. Valeri, The role of humidity and oxygen on MoS2 thin films deposited by RF PVD magnetron sputtering, Surf. Coat. Technol. 319 (2017) 345–352, https://doi.org/10.1016/j.surfcoat.2017.04.006.
[24] E. Serpini, A. Rota, S. Valeri, E. Ukraintsev, B. Rezek, T. Polcar, P. Nicolini, Nanoscale frictional properties of ordered and disordered MoS2, Tribol. Int. 136 (2019) 67–74, https://doi.org/10.1016/j.triboint.2019.03.004.

[25] D. Berman, S.A. Deshmukh, S.K.R.S. Sankaranarayanan, A. Erdemir, A.V. Sumant, Macroscale superlubricity enabled by graphene nanoscroll formation, Science 348 (2015) 1118–1122, https://doi.org/10.1126/science.1262024.
[26] B. Jiang, Z. Zhao, Z. Gong, D. Wang, G. Yu, J. Zhang, Superlubricity of metal-metal interface enabled by graphene and MoWS4 nanosheets, Appl. Surf. Sci. 520 (2020) 146303, https://doi.org/10.1016/j.apsusc.2020.146303.
[27] Z. Gong, J. Shi, B. Zhang, J. Zhang, Graphene nano scrolls responding to superlow friction of amorphous carbon, Carbon 116 (2017) 310–317, https://doi.org/10.1016/j.carbon.2017.01.106.
[28] R. Li, X. Yang, D. Hou, Y. Wang, J. Zhang, Superlubricity of carbon nanostructural films enhanced by graphene nanoscrolls, Mater. Lett. 271 (2020) 127748, https://doi.org/10.1016/j.matlet.2020.127748.
[29] F. Zhao, H. Li, L. Ji, Y. Wang, X. Liu, H. Zhou, J. Chen, Effect of microstructural evolution on mechanical and tribological properties of Ti-doped DLC films: how was an ultralow friction obtained? J. Vac. Sci. Technol. A 34 (2016) 031504 https://doi.org/10.1116/1.4944053.
[30] R. Li, X. Yang, Y. Wang, J. Zhang, J. Li, Graphitic encapsulation and electronic shielding of metal nanoparticles to achieve metal–carbon interfacial superlubricity, ACS Appl. Mater. Interfaces 13 (2021) 3397–3407, https://doi.org/10.1021/acsami.0c18900.
[31] D. Marchetto, P. Restuccia, A. Ballestrazzi, M.C. Righi, A. Rota, S. Valeri, Surface passivation by graphene in the lubrication of iron: a comparison with bronze, Carbon 116 (2017) 375–380, https://doi.org/10.1016/j.carbon.2017.02.011.
[32] R. Buzio, A. Gerbi, S. Uttiya, C. Bernini, A.E. Del Rio Castillo, F. Palazon, A.S. Siri, V. Pellegrini, L. Pellegrino, F. Bonaccorso, Ultralow friction of ink-jet printed graphene flakes, Nanoscale 9 (2017) 7612–7624, https://doi.org/10.1039/C7NR00625J.
[33] R. Buzio, A. Gerbi, C. Bernini, L. Repetto, A. Silva, A. Vanossi, Dissipation mechanisms and superlubricity in solid lubrication by wet-transferred solution-processed graphene flakes: implications for micro electromechanical devices, ACS Appl. Nano Mater. 6 (2023) 11443–11454, https://doi.org/10.1021/acsanm.3c01477.
[34] A.C. Ferrari, J. Robertson, Interpretation of Raman spectra of disordered and amorphous carbon, Phys. Rev. B 61 (2000) 14095–14107, https://doi.org/10.1103/PhysRevB.61.14095.
[35] C. Casiraghi, A.C. Ferrari, J. Robertson, Raman spectroscopy of hydrogenated amorphous carbons, Phys. Rev. B 72 (2005) 085401, https://doi.org/10.1103/PhysRevB.72.085401.
[36] X. Fan, L. Gu, S. Zeng, L. Zhu, C. Wang, Y. Wang, B. Zou, W. Huang, X. Chen, Z. S. Khan, X. Cao, Improving stability of thermal barrier coatings on magnesium alloy with electroless plated Ni–P interlayer, Surf. Coat. Technol. 206 (2012) 4471–4480, https://doi.org/10.1016/j.surfcoat.2012.05.004.
[37] A. Hadipour, S.M. Monirvaghefi, M.E. Bahrololoom, Electroless deposition of graded Ni–P coatings, Surf. Eng. 31 (2015) 399–405, https://doi.org/10.1179/1743294414Y.0000000430.
[38] P. Huang, W. Qi, X. Yin, J. Choi, X. Chen, J. Tian, J. Xu, H. Wu, J. Luo, Ultra-low friction of a-C:H films enabled by lubrication of nanodiamond and graphene in ambient air, Carbon 154 (2019) 203–210, https://doi.org/10.1016/j.carbon.2019.08.010.
[39] K.C. Mutyala, G.L. Doll, J. Wen, A.V. Sumant, Superlubricity in rolling/sliding contacts, Appl. Phys. Lett. 115 (2019) 103103, https://doi.org/10.1063/1.5116142.
[40] P. Wu, X. Chen, C. Zhang, J. Luo, Synergistic tribological behaviors of graphene oxide and nanodiamond as lubricating additives in water, Tribol. Int. 132 (2019) 177–184, https://doi.org/10.1016/j.triboint.2018.12.021.
[41] Z. Gong, C. Bai, L. Qiang, K. Gao, J. Zhang, B. Zhang, Onion-like carbon films endow macro-scale superlubricity, Diam. Relat. Mater. 87 (2018) 172–176, https://doi.org/10.1016/j.diamond.2018.06.004.
[42] W. Zhao, F. Duan, Friction properties of carbon nanoparticles (nanodiamond and nanoscroll) confined between DLC and a-SiO2 surfaces, Tribol. Int. 145 (2020) 106153, https://doi.org/10.1016/j.triboint.2019.106153.
[43] T.W. Scharf, I.L. Singer, Quantification of the thickness of carbon transfer films using Raman tribometry, Tribol. Lett. 14 (n.d.) 137–145. https://doi.org/10.1023/A:1021942822261.
[44] T.-B. Ma, Y.-Z. Hu, H. Wang, Molecular dynamics simulation of shear-induced graphitization of amorphous carbon films, Carbon 47 (2009) 1953–1957, https://doi.org/10.1016/j.carbon.2009.03.040.
[45] D.-S. Wang, S.-Y. Chang, Y.-C. Huang, J.-B. Wu, H.-J. Lai, M.-S. Leu, Nanoscopic observations of stress-induced formation of graphitic nanocrystallites at amorphous carbon surfaces, Carbon 74 (2014) 302–311, https://doi.org/10.1016/j.carbon.2014.03.035.
[46] T. Tokoroyama, C. Fujiwara, M. Murashima, M. Yamaguchi, N. Umehara, Effect of the graphite domain direction on the friction coefficient of tetrahedral amorphous carbon nitride, Diam. Relat. Mater. 143 (2024) 110853, https://doi.org/10.1016/j.diamond.2024.110853.
[47] A.C. Ferrari, J. Robertson, Raman spectroscopy of amorphous, nanostructured, diamond–like carbon, and nanodiamond, Philos. Trans. R. Soc. London, Ser. A 362 (2004) 2477–2512, https://doi.org/10.1098/rsta.2004.1452.
[48] G.N. Yushin, S. Osswald, V.I. Padalko, G.P. Bogatyreva, Y. Gogotsi, Effect of sintering on structure of nanodiamond, Diam. Relat. Mater. 14 (2005) 1721–1729, https://doi.org/10.1016/j.diamond.2005.06.030.
[49] F. Klauser, D. Steinmüller-Nethl, R. Kaindl, E. Bertel, N. Memmel, Raman studies of nano- and ultra-nanocrystalline diamond films grown by hot-filament CVD, Chem. Vap. Depos. 16 (2010) 127–135, https://doi.org/10.1002/cvde.200906827.
[50] V. Thapliyal, M.E. Alabdulkarim, D.R. Whelan, B. Mainali, J.L. Maxwell, A concise review of the Raman spectra of carbon allotropes, Diam. Relat. Mater. 127 (2022) 109180, https://doi.org/10.1016/j.diamond.2022.109180.
[51] V.N. Mochalin, O. Shenderova, D. Ho, Y. Gogotsi, The properties and applications of nanodiamonds, Nature Nanotech. 7 (2012) 11–23, https://doi.org/10.1038/nnano.2011.209.
[52] V.I. Korepanov, H. Hamaguchi, E. Osawa, V. Ermolenkov, I.K. Lednev, B.J. M. Etzold, O. Levinson, B. Zousman, C.P. Epperla, H.-C. Chang, Carbon structure in nanodiamonds elucidated from Raman spectroscopy, Carbon 121 (2017) 322–329, https://doi.org/10.1016/j.carbon.2017.06.012.
[53] M. Popov, V. Churkin, A. Kirichenko, V. Denisov, D. Ovsyannikov, B. Kulnitskiy, I. Perezhogin, V. Aksenenkov, V. Blank, Raman spectra and bulk modulus of nanodiamond in a size interval of 2–5 nm, Nanoscale Res. Lett. 12 (2017) 561, https://doi.org/10.1186/s11671-017-2333-0.
[54] D.M. Jang, Y. Myung, H.S. Im, Y.S. Seo, Y.J. Cho, C.W. Lee, J. Park, A.-Y. Jee, M. Lee, Nanodiamonds as photocatalysts for reduction of water and graphene oxide, Chem. Commun. 48 (2012) 696–698, https://doi.org/10.1039/C1CC16210A.
[55] I. Bydzovska, E. Shagieva, I. Gordeev, O. Romanyuk, Z. Nemeckova, J. Henych, L. Ondic, A. Kromka, S. Stehlik, Laser-induced modification of hydrogenated detonation nanodiamonds in ethanol, Nanomaterials 11 (2021) 2251, https://doi.org/10.3390/nano11092251.
[56] O.S. Kudryavtsev, R.H. Bagramov, D.G. Pasternak, A.M. Satanin, O.I. Lebedev, V. P. Filonenko, I.I. Vlasov, Raman fingerprints of ultrasmall nanodiamonds produced from adamantane, Diam. Relat. Mater. 133 (2023) 109770, https://doi.org/10.1016/j.diamond.2023.109770.